

# Hydrogel Transformed from Nanoparticles for Prevention of Tissue Injury and Treatment of Inflammatory Diseases

Zimeng Li, Gang Li, Jiajia Xu, Chenwen Li, Songling Han, Chunfan Zhang, Peng Wu, Yongyao Lin, Chenping Wang, Jianxiang Zhang,\* and Xiaodong Li\*

Functional hydrogels responsive to physiological and pathological signals have extensive biomedical applications owing to their multiple advanced attributes. Herein, engineering of functional hydrogels is reported via transformable nanoparticles in response to the physiologically and pathologically acidic microenvironment. These nanoparticles are assembled by a multivalent hydrophobic, pH-responsive cyclodextrin host material and a multivalent hydrophilic guest macromolecule. Driven by protons, the pH-responsive host-guest nanoparticles can be transformed into hydrogel, resulting from proton-triggered hydrolysis of the host material, generation of a hydrophilic multivalent host compound, and simultaneously enhanced inclusion interactions between host and guest molecules. By in situ forming a hydrogel barrier, the orally delivered transformable nanoparticles protect mice from ethanol- or drug-induced gastric injury. In addition, this type of nanoparticles can serve as responsive and transformable nanovehicles for therapeutic agents to achieve triggerable and sustained drug delivery, thereby effectively treating typical inflammatory diseases, including periodontitis and arthritis in rats. With combined advantages of nanoparticles and hydrogels, together with their good in vivo safety, the engineered transformable nanoparticles hold great promise in tissue injury protection and site-specific/local delivery of molecular and cellular therapeutic agents.

Hydrogels can be formed via physical entanglement, noncovalent interactions, and chemical cross-linking. By rational design at the molecular level, enhanced physicochemical properties, such as shear thinning, self-healing, and responsive capacities may be afforded to hydrogels. Of note, considerable efforts have been devoted to engineering stimuli-responsive hydrogels,<sup>[2]</sup> since their formation, degradation, multiscale shape, architecture, and functions can be easily and precisely manipulated via different physical, chemical, and biological signals in spatiotemporally controlled and/or programmed manners. In this aspect, different exogenous and endogenous bio-physicochemical triggers are generally utilized to precisely control hydrogel formation/degradation, finely tune the mechanics of hydrogels, and dynamically modulate hydrogel microenvironment.<sup>[2d,3]</sup> Hydrogels responsive to temperature, light, electrical/magnetic fields, ultrasound, mechanical forces, pH, redox potentials, and biochemical agents have been extensively examined for on-demand therapeutic

delivery of drugs and cells to treat different acute and chronic diseases,<sup>[3a,4]</sup> for which controlled release of molecular and cellular payloads is mainly achieved by triggering transitions between hydrogel and solution phases or hydrogels and solid states. Also, stimuli-responsive hydrogels have been

## 1. Introduction

Functional hydrogels have widespread applications in many fields, including drug delivery, cell therapy, tissue engineering, medical implants, soft electronics, biosensors, and actuators.<sup>[1]</sup>

Z. Li, J. Xu, X. Li  
Stomatology Hospital  
School of Stomatology  
Zhejiang University School of Medicine  
Zhejiang Provincial Clinical Research Center for Oral Diseases  
Key Laboratory of Oral Biomedical Research of Zhejiang Province  
Cancer Center of Zhejiang University  
Hangzhou 310006, P. R. China  
E-mail: cisarli@zju.edu.cn

G. Li, C. Li, C. Zhang, P. Wu, Y. Lin, C. Wang, J. Zhang  
Department of Pharmaceutics  
College of Pharmacy  
Third Military Medical University (Army Medical University)  
Chongqing 400038, P. R. China  
E-mail: jxzhang@tmmu.edu.cn

 The ORCID identification number(s) for the author(s) of this article can be found under <https://doi.org/10.1002/adma.202109178>.

S. Han, J. Zhang  
State Key Laboratory of Trauma  
Burn and Combined Injury  
Institute of Combined Injury  
Third Military Medical University (Army Medical University)  
Chongqing 400038, P. R. China

P. Wu  
College of Pharmacy and Medical Technology  
Hanzhong Vocational and Technical College  
Hanzhong, Shaanxi 723000, P. R. China

DOI: 10.1002/adma.202109178

applied as functional scaffolds of stem cells or progenitor cells for tissue engineering and regeneration.<sup>[4b,c,g,5]</sup> In this case, local microenvironments can be precisely modulated by biochemical/biophysical signals in situ or remote physical triggers to regulate cell fate and activity.<sup>[2e,5c,d]</sup> In addition, responsive hydrogels were developed to promote wound healing or inhibit postoperative tissue adhesion.<sup>[4a,g,5b,6]</sup>

The abovementioned functional hydrogels have demonstrated superior advantages in the management of a plethora of diseases or disorders. Despite these notable advances, further broadened applications of responsive hydrogels require innovative engineering of diverse parameters, such as regulatable gelation via physiological or pathological cues, shape/structure manipulation across multiple length scales, biocompatible hydrogel-forming materials, efficient incorporation of various types of therapeutics, controlled/sustained release of molecular

and cellular payloads, and spatiotemporal presentation of bioactive moieties.<sup>[1c,d,i,7]</sup>

Herein, we propose a new strategy for engineering functional hydrogels via stimuli-responsive transformation of nanoparticles (Figure 1a). As a concept of proof, transformable nanoparticles were designed and developed by self-assembly of a multivalent, hydrophobic, proton-sensitive host material and a multivalent hydrophilic guest macromolecule. Under acidic conditions, the pH-responsive guest transforming nanoparticles can be hydrolyzed to liberate hydrophilic multivalent host molecules, which can spontaneously assemble with the multivalent guest via enhanced host-guest interactions to give rise to hydrogel. The hydrogel-transformable nanoparticles effectively protected mice from ethanol- or drug-induced gastric injury, resulting from physiologically triggered in situ formation of protective hydrogel barriers on the stomach mucosa. Moreover,

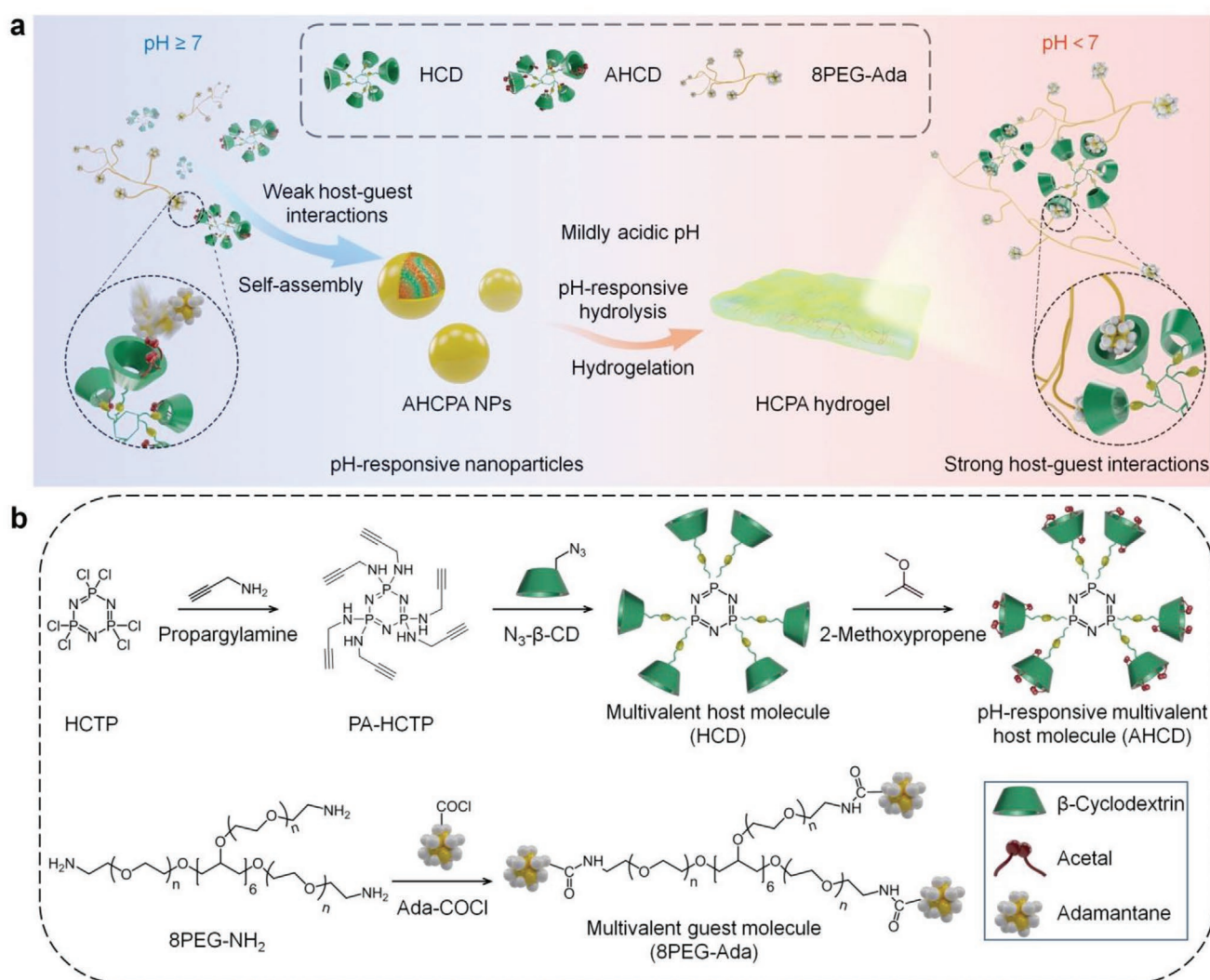


**Figure 1.** Design and synthesis of pH-triggerable hydrogel-transforming nanoparticles based on host-guest recognition. a) Schematic illustration of host-guest-interaction-mediated self-assembly of pH-responsive nanoparticles and acid-triggerable hydrogel transformation. b) A sketch showing the chemical structure and synthesis of multivalent host and guest molecules. HCTP, cyclic hexachlorocyclotriphosphazene; PA-HCTP, propargylamine-conjugated HCTP;  $N_3$ - $\beta$ -CD, mono-6-azido- $\beta$ -cyclodextrin; HCD,  $\beta$ -cyclodextrin-conjugated HCTP; AHCD, acetalated HCD; 8PEG-NH<sub>2</sub>, 8-arm poly(ethylene glycol) amine; Ada-COCl, 1-adamantanecarbonyl chloride; 8PEG-Ada, 8-arm poly(ethylene glycol) conjugated with adamantane; AHCPA NPs, nanoparticles assembled by AHCD and 8PEG-Ada; HCPA hydrogel, host-guest hydrogel formed by pH-triggered transformation of AHCPA NPs.

proton-driven hydrogel transformation of our pH-responsive nanoparticles can be triggered by inflammatory microenvironments (i.e., pathological cues), and therefore the transformable nanoparticles can serve as functional nanovehicles for different therapeutic agents to treat inflammatory diseases.

## 2. Results and Discussion

### 2.1. Synthesis and Characterization of Hydrophilic Multivalent Host and Guest Molecules

To demonstrate our hypothesis,  $\beta$ -cyclodextrin ( $\beta$ -CD) was employed as a functional moiety to engineer a multivalent host molecule (termed as HCD), due to its good biocompatibility and desirable affinity to a diverse array of guest molecules.<sup>[8]</sup> HCD was synthesized by conjugating  $\beta$ -CD onto hexachlorocyclotriphosphazene (HCTP) via click chemistry reaction (Figure 1b). To this end, 6 alkyne units were first introduced onto HCTP by nucleophilic reaction between propargyl amine (PA) and HCTP. The obtained compound PA-HCTP was characterized with <sup>1</sup>H NMR, <sup>31</sup>P NMR, and Fourier transform infrared (FT-IR) spectroscopy (Figure S1a–c, Supporting Information), which was further confirmed by matrix-assisted laser desorption/ionization-time of flight (MALDI-TOF) mass spectrometry (Figure S1d, Supporting Information). Then, HCD was obtained by click reaction between PA-HCTP and mono-6-azido- $\beta$ -CD ( $N_3$ - $\beta$ -CD), and its successful synthesis was affirmed by FT-IR, <sup>1</sup>H NMR, and MALDI-TOF spectra (Figure S2, Supporting Information). Further elemental analysis revealed  $\approx 4$ – $5$   $\beta$ -CD units in each HCD molecule, well consistent with the result based on MALDI-TOF mass spectrometry (Figure S2c, Supporting Information). On the other hand, a multivalent guest polymer (8PEG-Ada) was prepared by conjugating adamantly (Ada) moieties onto 8-arm poly(ethylene glycol) (8PEG) via condensation reaction between formyl chloride and amine groups (Figure 1b). <sup>1</sup>H NMR spectroscopy indicated that nearly 100% of terminal hydroxyl groups of 8PEG were functionalized with Ada moieties (Figure S3a, Supporting Information). Through a similar synthetic route, cyanine5 (Cy5)-labeled 8PEG-Ada (i.e., 8PEG-Ada-Cy5) was synthesized, with each 8PEG containing one Cy5 moiety (Figure S3b, Supporting Information).

### 2.2. Host-Guest Hydrogels Assembled by HCD and 8PEG-Ada

We then examined whether host-guest hydrogels can be assembled by the newly synthesized multivalent host and guest molecules. Measurement by isothermal titration calorimetry (ITC) revealed strong binding affinity between HCD and 8PEG-Ada in deionized water (Figure S4a, Supporting Information). The quantified binding constant was  $4.6 \times 10^5 \text{ M}^{-1}$ , which is notably higher than that between free  $\beta$ -CD and 1-adamantanecarboxylate in aqueous solution (i.e.,  $8.5 \times 10^4 \text{ M}^{-1}$ ) (Figure S4b, Supporting Information). This suggested that host-guest interactions between multivalent host and guest molecules can be considerably enhanced, as compared to those of the corresponding monovalent systems. Of note, pH and ionic strength had no significant effects on binding constants between HCD and 8PEG-Ada (Figure S5, Supporting Information).

Subsequently, we tested hydrogel formation capability of HCD/8PEG-Ada at various molar ratios of  $\beta$ -CD to Ada by rheological studies. At a  $\beta$ -CD/Ada ratio of 1:0.25, both direct observation and quantification of frequency-dependent storage modulus ( $G'$ ) and loss modulus ( $G''$ ) values of aqueous solution containing HCD and 8PEG-Ada indicated no hydrogel formation (Figure 2a). By contrast, stable hydrogels were obtained for aqueous solutions containing HCD/8PEG-Ada at 1:0.5, 1:1, and 1:2, as implicated by digital photos and higher  $G'$  relative to  $G''$  values (Figure 2b–d). Particularly, hydrogel with the highest modulus was formed by HCD/8PEG-Ada at 1:1, showing slight changes in  $G'$  values with increasing frequency. Nevertheless, hydrogel could not be formed at the  $\beta$ -CD/Ada molar ratio of 1:4 (Figure 2e). These results suggested that mismatched host/guest moieties at higher contents of either  $\beta$ -CD or Ada moieties are not beneficial for self-assembly of host-guest hydrogels. Also, hydrogelation of HCD/8PEG-Ada is closely related to their solid content. At the  $\beta$ -CD/Ada ratio of 1:1, only viscous solutions were observed when the solid content was 4% or 6%, while hydrogelation occurred at the solid contents  $\geq 8\%$  (Figure S6, Supporting Information). For the HCD/8PEG-Ada hydrogel at the  $\beta$ -CD/Ada ratio of 1:1 and with a solid content of 10%, in vitro tests in simulated gastric fluid (SGF) indicated that its maximal swelling can be achieved within 5 min (Figure S7a, Supporting Information). Also, in vitro degradation experiments showed that this hydrogel was stable in SGF (Figure S7b, Supporting Information), agreeing with the finding that pH and ionic strength exhibited negligible impact on the binding constant of HCD/8PEG-Ada (Figure S5, Supporting Information). Collectively, these results demonstrated that hydrogels can be successfully assembled by our newly synthesized multivalent host and guest molecules, and the properties of thus engineered hydrogels can be fine-tuned by varying their ratios or contents.

### 2.3. Engineering of pH-Triggerable Host-Guest Nanoparticles

To develop transformable nanoparticles capable of gelating via host-guest complexation upon pH triggering, HCD was first acetalated to produce acid-labile materials (Figure 1b). By regulating the acetalation time, acetalated HCD materials (i.e., AHCDs) with varied acetalation degrees were obtained (Figure S8, Supporting Information), as indicated by gradually increased methyl proton signals in <sup>1</sup>H NMR spectra. AHCDs collected after acetalation for 15, 30, 60, and 120 min are defined as AHCD15, AHCD30, AHCD60, and AHCD120, respectively. As expected, real-time <sup>1</sup>H NMR spectroscopy revealed triggerable hydrolysis of different AHCDs at pH 1 (Figure 2f–i), showing complete hydrolysis within 10, 15, 20, and 25 min for AHCD15, AHCD30, AHCD60, and AHCD120, respectively. This is due to varied acetalation degrees for different AHCDs (Figure S8b, Supporting Information). On the other hand, this difference in the hydrolysis rate can be attributed to the relative contents of cyclic and linear acetals. As previously reported, short acetalation time may afford materials with relatively high contents of linear acetal that generally displays more rapid hydrolysis as compared to cyclic acetal.<sup>[9]</sup> Of note, complete hydrolysis of AHCDs gave rise to HCD and other water soluble byproducts.

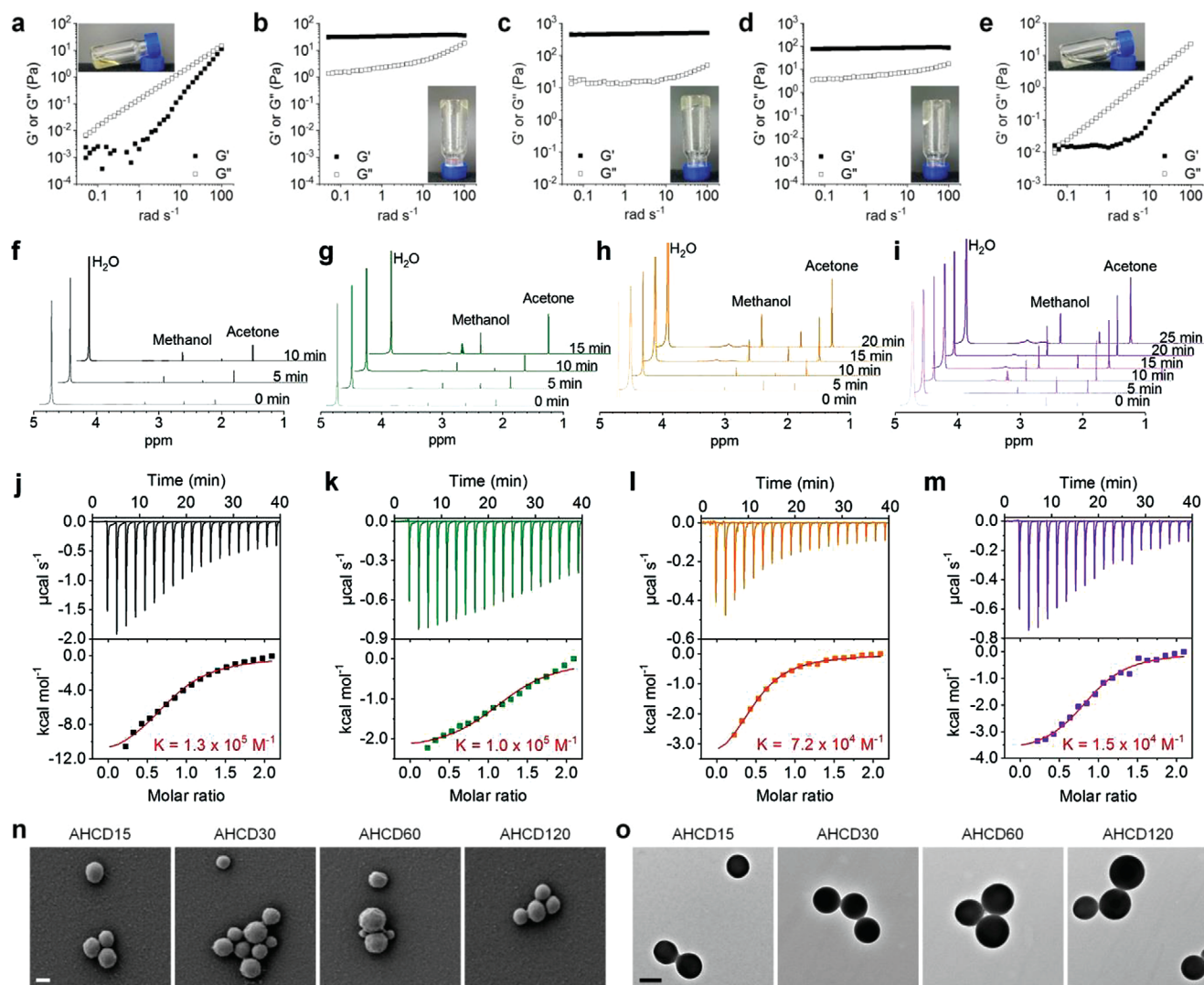


**Figure 2.** Characterization of host-guest hydrogels and pH-responsive host-guest nanoparticles. a–e) Rheological properties of aqueous solutions containing a multivalent host molecule (HCD) and a multivalent guest molecule (8PEG–Ada) at  $\beta$ -CD/Ada molar ratios of 1:0.25 (a), 1:0.5 (b), 1:1 (c), 1:2 (d), and 1:4 (e).  $G'$ , storage modulus;  $G''$ , loss modulus. f–i)  $^1\text{H}$  NMR spectra showing time-dependent hydrolysis of different acetalated HCD (i.e., AHCD) materials of AHCD15 (f), AHCD30 (g), AHCD60 (h), and AHCD120 (i) in  $\text{D}_2\text{O}$  at pH 1. AHCD15, AHCD30, AHCD60, and AHCD120 denote AHCD with acetalation reaction times of 15, 30, 60, and 120 min, respectively. j–m) ITC curves and quantified binding constants showing host-guest interactions between 8PEG–Ada and AHCD15 (j), AHCD30 (k), AHCD60 (l), or AHCD120 (m). n, o) SEM (n) and TEM (o) images of nanoparticles assembled by 8PEG–Ada and different AHCD materials. Scale bars, 200 nm.

In addition, ITC measurement revealed the presence of host-guest interactions between different AHCDs and 8PEG–Ada (Figure 2j–m). Nevertheless, the binding constant of AHCDs/8PEG–Ada gradually decreased for AHCD15, AHCD30, AHCD60, and AHCD120, which was  $1.3 \times 10^5$ ,  $1.0 \times 10^5$ ,  $7.2 \times 10^4$ , and  $1.5 \times 10^4 \text{ M}^{-1}$ , respectively. This is in line with the fact that prolonged acetalation time leads to the increased acetalation degree,<sup>[9b]</sup> while the introduced acetal moieties can partly cover the cavity of  $\beta$ -CD,<sup>[10]</sup> thereby impairing the binding affinity between AHCDs and 8PEG–Ada. We then prepared pH-responsive nanoparticles based on AHCDs/8PEG–Ada by nanoprecipitation in combination with host-guest self-assembly. To this end, AHCDs in dimethyl sulfoxide was slowly added into aqueous solution of 8PEG–Ada. Regardless of different

AHCDs with varied acetalation degrees, spontaneous host-guest recognition led to well-defined spherical nanoparticles, as illustrated by both scanning electron microscopy (SEM) and transmission electron microscopy (TEM) images (Figure 2n,o). Characterization via dynamic light scattering revealed relatively narrow size distribution for all AHCDs/8PEG–Ada assembled nanoparticles, with mean diameter of  $150 \pm 40 \text{ nm}$  and negative  $\zeta$ -potential (Figure S9, Supporting Information). For different nanoparticles, their elemental composition was further confirmed by energy dispersive X-ray spectroscopy (Figure S10, Supporting Information).

Hydrophobicity of AHCDs and impaired host-guest interactions between AHCDs and 8PEG–Ada should mainly contribute to the formation of AHCDs/8PEG–Ada nanoparticles

in neutral aqueous solutions, since they can lead to considerably low degrees of cross-linking due to aggregation of AHCDs via hydrophobic interactions. In this aspect, 8PEG-Ada can function as a surfactant to stabilize hydrophobic AHCD-derived nanoaggregates by relatively weak host-guest interactions (most probably together with hydrophobic forces), thereby resulting in the formation of spherical nanoparticles. In addition to ITC experiments (Figure 2j–m), the interactions between AHCD and 8PEG-Ada were verified by FT-IR spectroscopy (Figure S11, Supporting Information). Consistent with pH-responsive hydrolysis behaviors of AHCDs, different AHCD/8PEG-Ada nanoparticles showed clearly pH-dependent hydrolysis profiles (Figure S12, Supporting Information). At examined pH values, nanoparticles derived from AHCD15 displayed the most rapid hydrolysis rate. Regardless of different nanoparticles, they all exhibited relatively good stability at pH 7.4, as implicated by time-dependent changes in hydrolysis degrees and mean diameters upon long-term incubation (Figure S12d,e, Supporting Information). For nanoparticles assembled by AHCD15 and 8PEG-Ada, *in vitro* tests in three cell lines (human gastric epithelial cells, human gingival fibroblasts, and ATDC-5 murine chondrocytes) revealed negligible cytotoxicity even after 24 h of incubation at  $800 \mu\text{g mL}^{-1}$  (Figure S13, Supporting

Information). Together, pH-responsive nanoparticles with tailorable hydrolysis profiles and good cytocompatibility can be engineered by host-guest-interaction-mediated assembly of AHCDs and 8PEG-Ada.

#### 2.4. Acid-Triggered Transformation of pH-Responsive Nanoparticles to Hydrogels

Considering rapid pH-responsive hydrolysis of nanoparticles assembled by AHCD15 and 8PEG-Ada (defined as AHCPA NPs), they were employed in following studies. Whereas hydrolysis of low concentrations of AHCPA NPs at pH 1 led to clear solutions, pH-triggered hydrogel formation was observed at high concentrations of AHCPA NPs (>10 wt%). For 10% AHCPA NPs, direct observation revealed the formation of hydrogel within a few seconds after incubation at pH 1 (Figure 3a), indicating successful transformation of AHCPA NPs into hydrogel (Figure 3b). This nanoparticle-to-hydrogel transformation was also confirmed by rheological measurement, as indicated by more rapidly increased  $G'$  relative to  $G''$  (Figure 3c). Similarly, the pH-triggered hydrogel formation was found for aqueous solutions of AHCPA NPs at pH

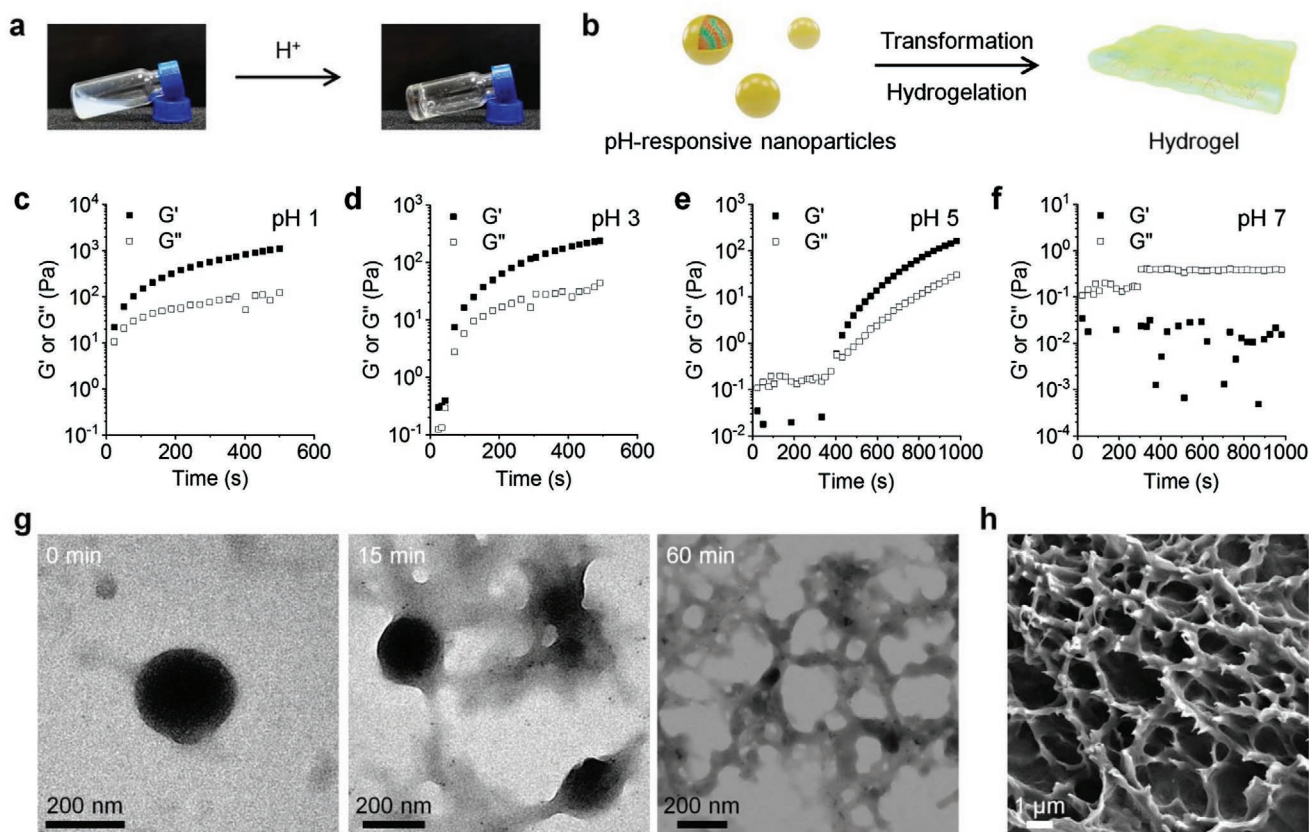


**Figure 3.** Characterization of *in vitro* transformation from nanoparticles to hydrogels upon pH triggering. a) Digital photos show transition of nanoparticles to hydrogel after incubation at pH 1 for 5 min. b) A sketch illustrates hydrogel transformation of pH-responsive nanoparticles. c–f) Oscillatory rheological characterization of pH-dependent transition of AHCPA NPs to hydrogels at pH 1 (c), pH 3 (d), pH 5 (e), or pH 7 (f). In all cases, the solid content was 10 wt%, while the molar ratio of  $\beta$ -CD/Ada was 1:1.  $G'$ , storage modulus;  $G''$ , loss modulus. The modulus transition time was 23, 70, and 403 s at pH 1, pH 3, and pH 5, respectively. g) STEM images of AHCPA NPs after incubation at pH 5 for 0, 15, or 60 min. h) A typical SEM image shows the cross-section structure of hydrogel transformed from AHCPA NPs at pH 5 after freeze-drying.

3 and pH 5 (Figure 3d,e), although relatively long time was required in these cases. For the transformed hydrogels at pH 1, 3, and 5, they reached the maximum  $G'$  after  $\approx 10$ , 20, and 60 min, respectively. Consistent with acid-responsive hydrolysis of AHCPA NPs, no hydrogel formation was observed at pH 7 (Figure 3f). Further, characterization via scanning transmission electron microscopy (STEM) was performed to provide detailed information regarding the transformation process at pH 5. Time-dependent STEM images clearly showed the disappearance of nanoparticles, but the appearance of network structures (Figure 3g). The typical network structure of hydrogel was also observed by SEM (Figure 3h). These results demonstrated that pH-responsive AHCPA NPs can be transformed into hydrogel upon acid triggering. This transformation is mainly attributed

to the generation of hydrophilic HCD molecules and simultaneously enhanced host–guest interactions.

Based on the above finding, we speculate that AHCPA NPs can be transformed into hydrogel in the stomach after oral administration (Figure 4a). To test this hypothesis, we examined gelation and retention profiles of orally delivered AHCPA NPs derived from AHCD15 and 8PEG–Ada–Cy5 (i.e., Cy5/AHCPA NPs). Nanoparticles based on acetalated  $\beta$ -CD and 8PEG–Ada–Cy5 (i.e., Cy5/ACPA NPs) were used as the control (Figure S14, Supporting Information), since  $\beta$ -CD and 8PEG–Ada cannot form a network structure to mediate the hydrogel formation. After oral gavage of Cy5/AHCPA NPs in mice, Cy5 fluorescence in the stomach was maintained for more than 2 h (Figure 4b,c). By contrast, Cy5 fluorescence notably

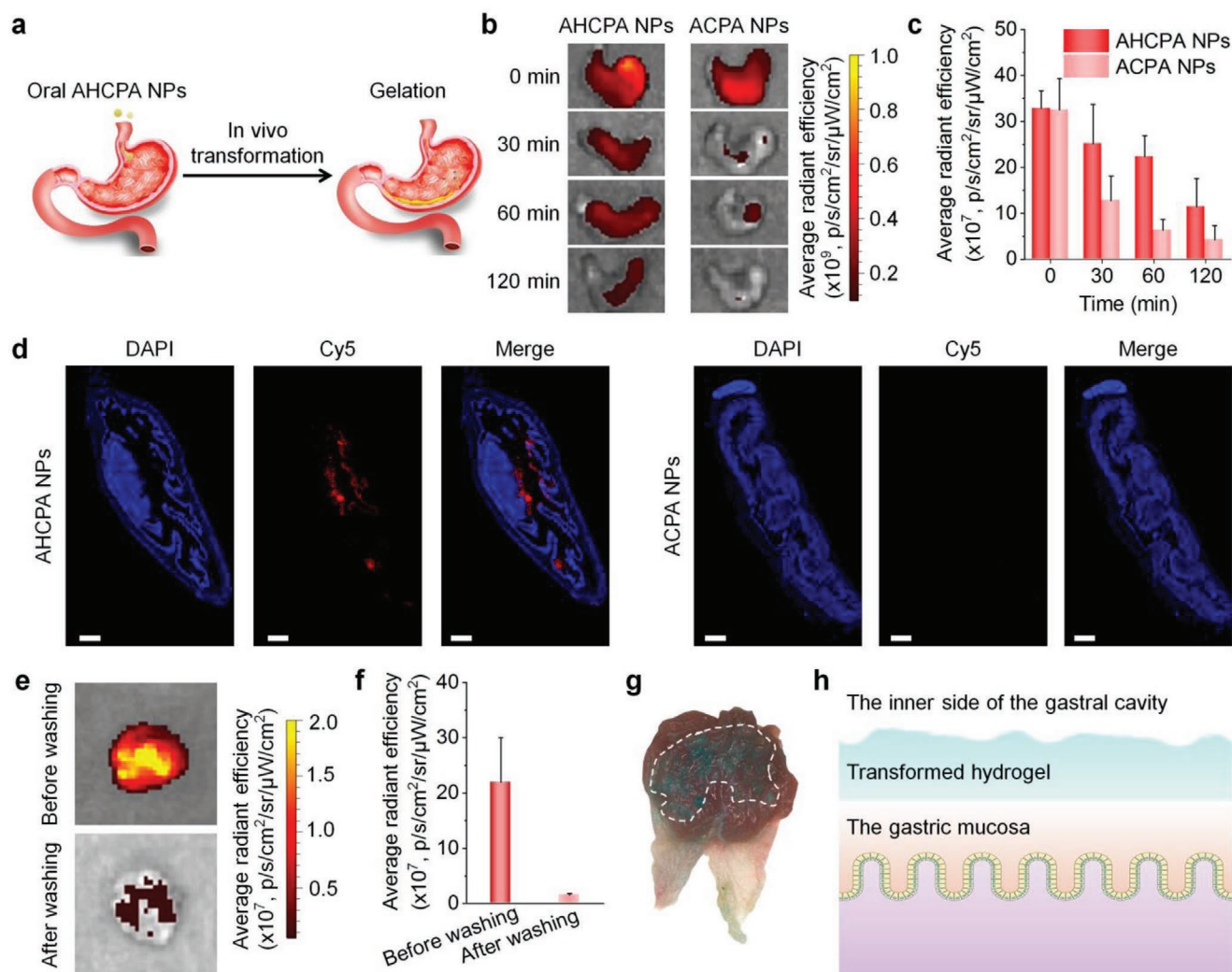


**Figure 4.** In vivo transformation of AHCPA NPs to hydrogels in the mouse stomach. a) Schematic illustration of in situ hydrogel formation in the stomach after oral administration of triggerable AHCPA NPs. b,c) Ex vivo images (b) and quantitative analysis (c) of Cy5-labeled AHCPA NPs or ACPA NPs in the mouse stomach after oral gavage. d) Confocal fluorescence images show the distribution of AHCPA-NP-derived hydrogel coating in the stomach at 1 h after oral gavage. Scale bars, 1 mm. e,f) Ex vivo imaging demonstrates physical coating of transformed hydrogel on the stomach mucosa. Ex vivo images (e) and quantitative data (f) show fluorescence intensities before and after washing of stomach tissues with PBS. g) A typical digital photo acquired by stereomicroscopy showing the presence of a hydrogel-like coating on the gastric mucosa after oral gavage of Cy5/AHCPA NPs. h) A sketch illustrating physical coating of transformed hydrogel on the gastric mucosa. Data are expressed as mean  $\pm$  standard deviation (s.d.) (c,  $n = 3$ ; f,  $n = 5$ ).

decreased even at 30 min after oral delivery of Cy5/ACPA NPs. Correspondingly, confocal microscopic observation clearly showed the fluorescence distribution on the gastric mucosal layer for mice treated with Cy5/AHCPA NPs (Figure 4d), while the Cy5/ACPA NP group displayed negligible fluorescence. Accordingly, the notably enhanced fluorescence retention after oral delivery of Cy5/AHCPA NPs suggested the formation of hydrogel that can delay excretion from the stomach. In addition, the gastric fluorescence of Cy5-/AHCPA-NP-treated mice was dramatically reduced after thorough rinsing of the opened stomach with phosphate-buffered saline (PBS) (Figure 4e,f). Moreover, a hydrogel-like coating on the gastric mucosa was directly observed by stereomicroscopy (Figure 4g). This is also consistent with the result that HCD/8PEG-Ada hydrogel is stable in SGF (Figure S7, Supporting Information). Together, these results indicated physical coating of the hydrogel formed by AHCPA NPs on the gastric mucosa (Figure 4h). The gastric retention time of AHCPA-NP-derived hydrogel is largely consistent with the lifetime of gastric mucus that is  $\approx 2\text{--}4$  h in mice as previously reported.<sup>[11]</sup> This fast turnover of gastric mucus is resulting from continuous secretion and clearance of its compositions.<sup>[12]</sup> As for orally delivered ACPA NPs, rapid hydrolysis followed by quick elimination from the stomach may occur due to peristaltic motion, digestion, and/or absorption. On the one hand, low pH in the mouse stomach, varying from 2.7 to 4.1,<sup>[13]</sup> is responsible for hydrogel formation from AHCPA NPs. On the other hand, the dilution effect after oral gavage can be neglected, since the water content in the stomach is only 0.1–0.3 mL for the fed and fasted mice.<sup>[13b]</sup> Taken together, these results substantiated that nanoparticle-to-hydrogel transformation can be successfully triggered for pH-responsive AHCPA NPs under both *in vitro* and *in vivo* conditions.

## 2.5. Protection of Gastric Injury by In Situ Transformed Hydrogel from AHCPA NPs

We then examined whether *in situ* transformed hydrogel based on orally delivered AHCPA NPs can protect the stomach from chemical/drug-induced injury. An ethanol-induced gastric injury model was first used (Figure S15a, Supporting Information). At 1 h after oral gavage of ethanol, stereomicroscopy observation revealed severe damage of the gastric mucosa for mice in the model group treated with PBS alone, as implicated by significant bleeding points (Figure S15b,c, Supporting Information). By contrast, pretreatment with AHCPA NPs via oral gavage at 1 h before exposure to ethanol almost completely prevented mice from ethanol-induced redness and swelling. Correspondingly, the model group showed abnormally increased gastric volume, an index of flatulence due to acute inflammation (Figure S15d, Supporting Information), which was effectively reduced by oral administration of AHCPA NPs prior to alcohol treatment. In addition, treatment with AHCPA NPs significantly decreased expression levels of typical proinflammatory cytokines, including tumor necrosis factor (TNF)- $\alpha$ , interleukin (IL)-1 $\beta$ , IL-6, and myeloperoxidase (MPO) in gastric tissue homogenates (Figure S15e–h, Supporting Information). Moreover, SEM observation indicated nearly normal microstructure of the gastric mucosa in the AHCPA NP group, which

is notably different from that of the model group (Figure S15i, Supporting Information). Further evaluation was performed by examination on histological sections stained with hematoxylin and eosin (H&E) or periodic acid–Schiff (PAS). The model group displayed notable damage of the gastric epithelial barrier and necrosis of epithelial cells (Figure S15j, Supporting Information), which are characteristic patterns of gastric mucosal injury. These histological abnormalities were considerably prevented by oral administration of transformable nanoparticles, as implicated by the intact mucosal layer as well as the absence of hemorrhage and necrosis.

Subsequently, protective effects of gel-transformable nanoparticles were also examined in mice with gastric ulcers induced via indomethacin (IND) (Figure 5a), a typical nonsteroidal anti-inflammatory drug (NSAID) frequently used for the treatment of osteoarthritis, rheumatoid arthritis, and ankylosing spondylitis.<sup>[14]</sup> In this case, preadministration of AHCPA NPs significantly inhibited bleeding, ulceration, body weight loss, and acute inflammatory responses resulting from IND stimulation (Figure 5b–h). Moreover, SEM observation and histological analysis of sections stained with H&E or PAS revealed considerably improved microstructure of the gastric mucosa and the maintained intact epithelial barrier by the orally delivered transformable nanoparticles (Figure 5i,j).

Taken together, these results substantiated that oral administration of pH-responsive AHCPA NPs can effectively prevent gastric injury by *in situ* forming a protective hydrogel layer. This type of transformable nanoparticles can serve as promising gastric mucosal protective agents for the prophylactic treatment of gastric injury resulting from alcohol consumption or applications of NSAIDs.

## 2.6. Treatment of Inflammatory Diseases with Drug-Loaded Transformable Nanoparticles

As well documented, acidosis is generally observed at inflamed sites of different acute and chronic inflammatory diseases.<sup>[15]</sup> To examine whether AHCPA NPs can also function as transformable nanovehicles of therapeutic agents for treating inflammatory diseases, dexamethasone (DEX) was used as a model anti-inflammatory drug. DEX-loaded AHCPA NPs were also prepared by the aforementioned nanoprecipitation/self-assembly method. The obtained DEX nanotherapy displayed a spherical shape and narrow size distribution (Figure S16a–c, Supporting Information), with the mean diameter of 146 nm, negative  $\zeta$ -potential, and the DEX loading content of 6.8%. *In vitro* release tests showed pH-triggerable drug release from DEX/AHCPA NPs (Figure S16d, Supporting Information), with rapid drug release at pH 6.5. Notably, DEX/AHCPA NPs displayed a dramatically slow release profile at pH 7.4. Besides the stability of AHCPA NPs at neutral pH levels (Figures S12d and S16e, Supporting Information), host–guest complexation between DEX and  $\beta$ -CD moieties may considerably delay drug release from AHCPA NPs (Figure S16f, Supporting Information). The host–guest-interaction-mediated delayed release of DEX was also reported for other  $\beta$ -CD-containing nanovehicles.<sup>[8e]</sup>

Initially, periodontitis, a representative chronic inflammatory disease triggered by microorganisms in the dental plaque,<sup>[16]</sup>

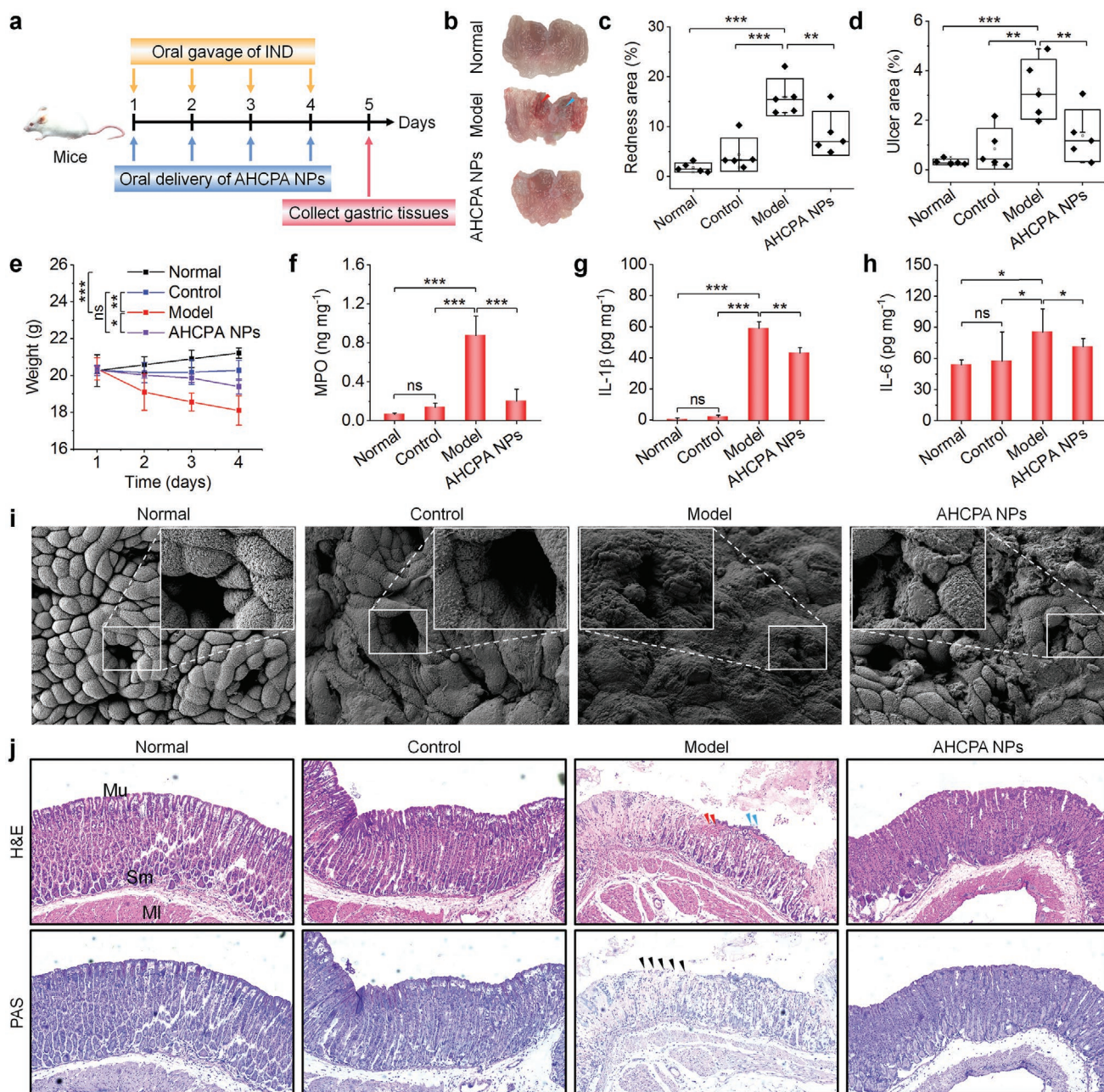


**Figure 5.** AHCPA NPs protected mice from indomethacin (IND)-induced gastric injury. a) Schematic illustration of the establishment of a mouse model of IND-induced gastric injury and treatment strategies. b–d) Representative digital photos show severe ulceration (b) and quantification of the relative area of redness (c) and ulcer (d) regions. Redness is indicated by red arrowheads, while ulcers are denoted by blue arrowheads. e) Body weight changes of mice after different treatments. f–h) The expression levels of MPO (f), IL-1 $\beta$  (g), and IL-6 (h) in gastric tissues. i) SEM images of the gastric antrum in different groups. Insets show high resolution images. j) Histological sections of gastric tissues stained with H&E (upper) or PAS (lower). Ulcers are indicated with red arrowheads, while inflammatory cells are illustrated with blue arrowheads. Loss of glycoproteins on the mucous membrane is denoted with black arrowheads. Mu, mucosa; Sm, submucosa; MI, muscularis. Normal, mice without any treatments; Control, healthy mice treated with the vehicle; Model, mice treated with IND at 16 mg kg<sup>-1</sup>; AHCPA NPs, mice simultaneously treated with AHCPA NPs and IND by oral gavage. Data in (e–h) are expressed as mean  $\pm$  s.d. ( $n = 5$ ). \* $p < 0.05$ , \*\* $p < 0.01$ , \*\*\* $p < 0.001$ ; ns, no significance.

was established in rats by a ligature-induced procedure.<sup>[17]</sup> Of note, local sucrose fermentation due to the presence of dental plaque in the periodontal pocket leads to a consistently acidic microenvironment (even  $< \text{pH } 5$ ).<sup>[18]</sup> Using Cy5/AHCPA NPs, we first demonstrated that locally delivered transformable

nanoparticles could be retained in the periodontal pocket of periodontitis rats for  $\approx 2$  days (Figure S17, Supporting Information). This is in accordance with the result based on rheological studies that AHCPA NPs can transform into hydrogel under pH conditions relevant to periodontitis (Figure 3e,g and

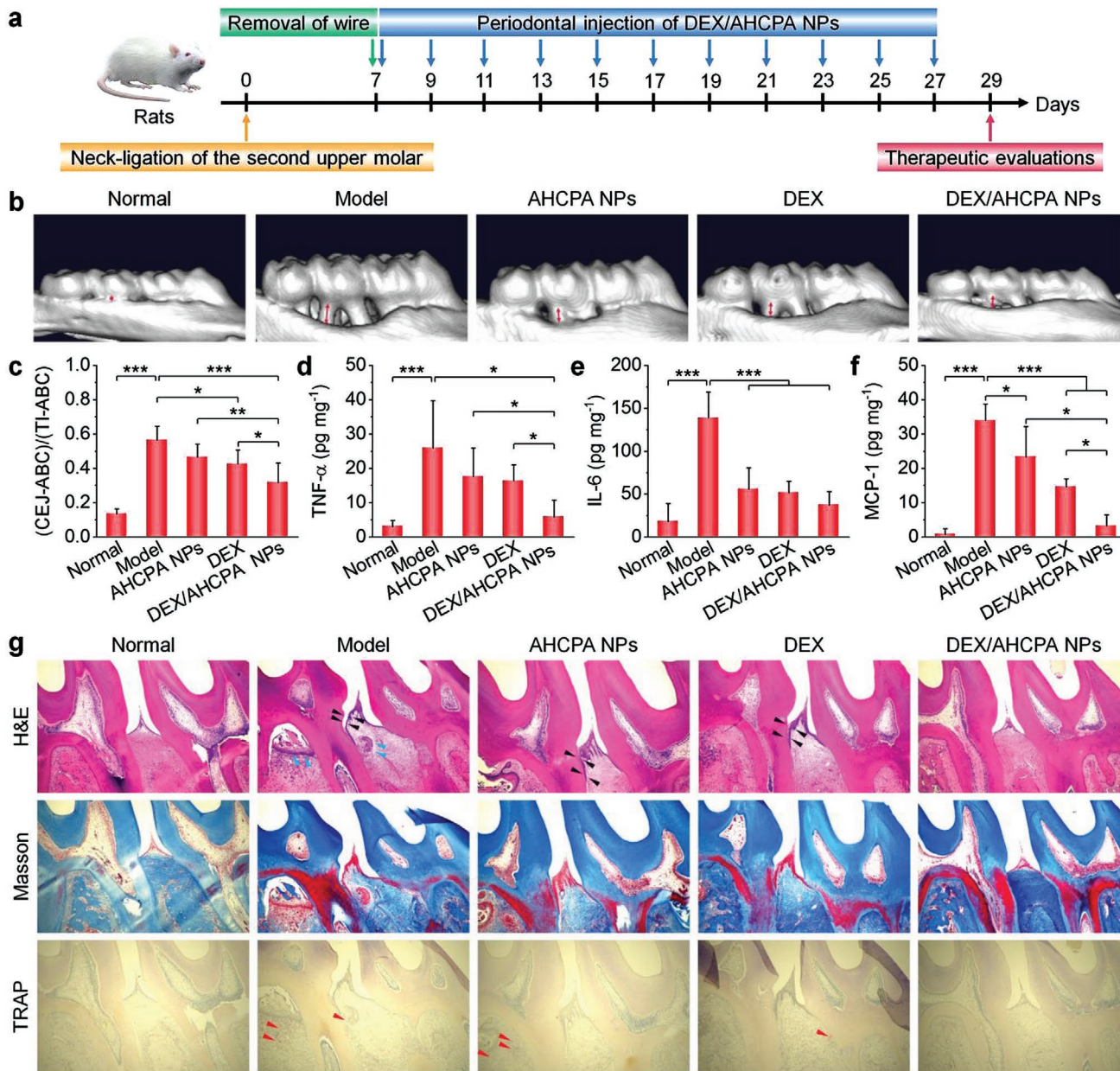


**Figure 6.** Treatment of periodontitis via triggerable AHCPA NPs containing an anti-inflammatory drug DEX. a) A sketch shows the establishment of periodontitis in rats and the related treatment regimens. b) Typical 3D micro-CT images of teeth and periodontal tissues of mice in different groups. The red lines with double arrowheads indicate the distance (termed as CEJ–ABC) from the cemento enamel junction (CEJ) to the alveolar bone crest (ABC). The distance between the teeth interface (TI) and the alveolar bone crest (ABC) is defined as TI–ABC. c) Quantification of the ratio of the height of the exposed root to the height of the entire tooth, which is denoted as (CEJ–ABC)/(TI–ABC). d–f) The expression levels of TNF- $\alpha$  (d), IL-6 (e), and MCP-1 (f) in the periodontium of rats subjected to different treatments. g) Typical histological sections of the periodontal tissues stained with H&E, Masson, or TRAP. Black arrowheads indicate periodontal pockets, blue arrowheads denote inflammatory cells, and red arrowheads show osteoclasts. Normal, rats without any treatments; Model, diseased rats subjected to ligation and local injection of PBS in the periodontal pocket; AHCPA NPs, diseased rats treated with AHCPA NP by local injection; DEX, diseased rats treated with free DEX; DEX/AHCPA NPs, diseased rats treated with DEX-loaded AHCPA NPs. Data in (c–f) are expressed as mean  $\pm$  s.d. ( $n = 5$ ). \* $p < 0.05$ , \*\* $p < 0.01$ , \*\*\* $p < 0.001$ .

Figure S18 (Supporting Information)). Then, *in vivo* therapeutic effects of DEX/AHCPA NPs were evaluated after local injection every two days (Figure 6a). At day 21 after different treatments, micro-computed tomography (micro-CT) scanning revealed considerable bone loss on the buccal side of rats in the model group (Figure 6b), while treatment with the

transformable nanotherapy notably attenuated this abnormal change. Further quantitative assessment by measuring the cemento enamel junction to the alveolar bone crest (CEJ–ABC) confirmed the beneficial outcome post treatment with DEX/AHCPA NPs (Figure 6c). The expressions of TNF- $\alpha$ , IL-6, and monocyte chemoattractant protein (MCP)-1 were also

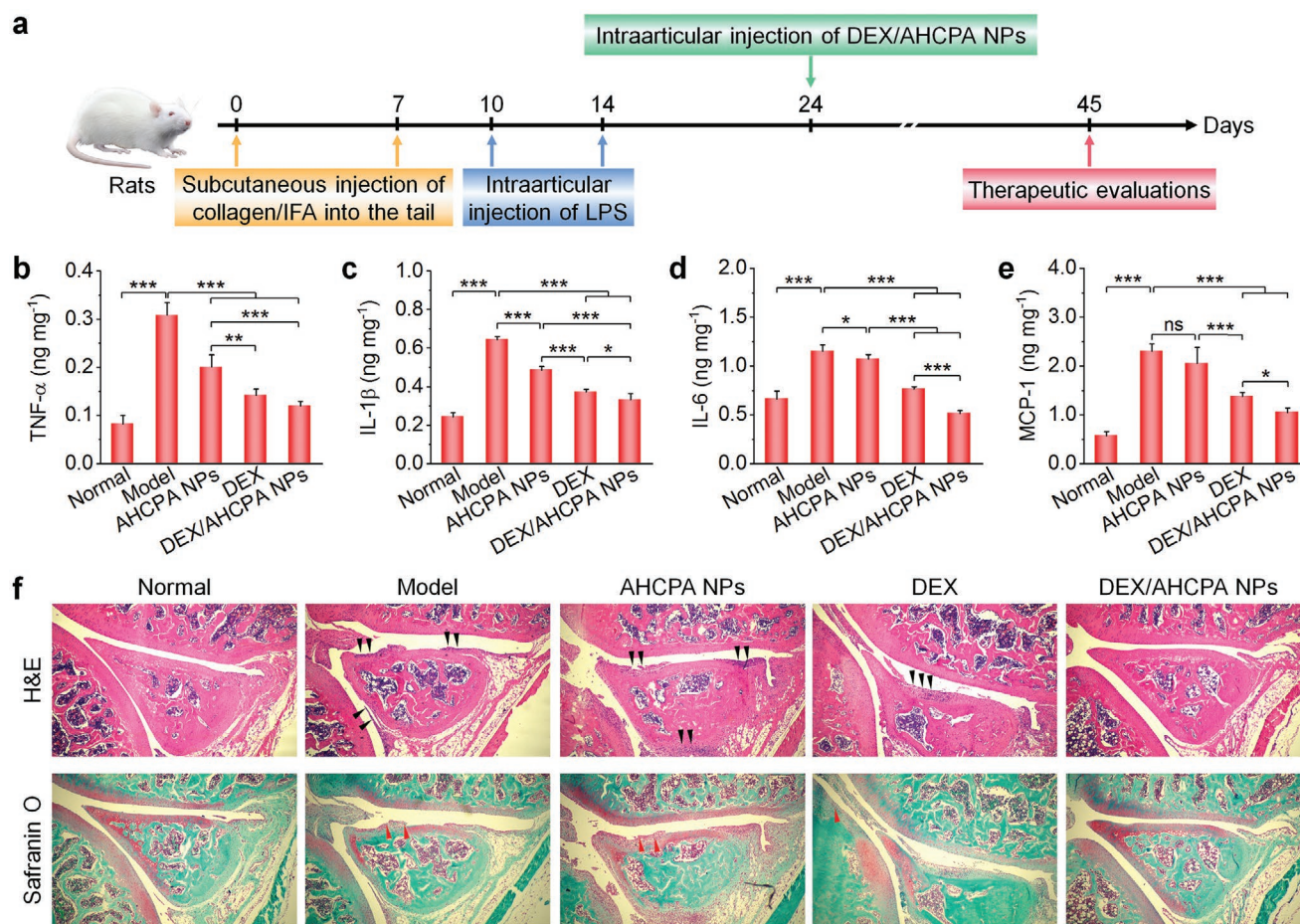


**Figure 7.** Treatment of arthritis with triggerable AHCPA NPs containing DEX. a) A workflow shows the establishment of a mouse model of collagen/LPS-induced arthritis and treatment regimens. b–e) The expression levels of TNF- $\alpha$  (b), IL-1 $\beta$  (c), IL-6 (d), and MCP-1 (e) in the joint capsule of mice after different treatments. f) Typical histological sections of the joint capsule stained with either H&E or Safranin O/Fast Green. The black arrowheads show the inflammatory sites. The damaged regions of cartilage are indicated with red arrowheads. Normal, healthy rats without any treatments; Model, rats subjected to subcutaneous injection of collagen emulsion into the tail and local injection of LPS into the joint capsule; AHCPA NPs, diseased rats treated with AHCPA NPs via local injection into the inflamed joint capsule; DEX, diseased rats treated with free DEX; DEX/AHCPA NPs, diseased rats treated with DEX-loaded AHCPA NPs. Data in (b–e) are expressed as mean  $\pm$  s.d. ( $n = 4$ ). \* $p < 0.05$ , \*\* $p < 0.01$ , \*\*\* $p < 0.001$ ; ns, no significance.

significantly suppressed by DEX/AHCPA NPs (Figure 6d–f). Whereas free DEX also displayed efficacies to certain degrees, the most significant therapeutic effects were achieved by the triggerable nanotherapy. Further inspection of histological sections stained with H&E, Masson, or tartrate resistant acid phosphatase (TRAP) revealed remarkably attenuated inflammatory infiltration as well as notably reduced bone absorption and formation of periodontal pockets after treatment with DEX/AHCPA NPs (Figure 6g).

Also, we examined therapeutic effects of the transformable DEX nanotherapy in a rat model of arthritis induced with collagen/lipopolysaccharide (LPS) (Figure 7a), since synovial fluid acidosis frequently occurs in arthritic knee joints, showing pH ranges of nearly 6.5–7.3.<sup>[15,19]</sup> Of note, we found that locally delivered transformable nanoparticles could be retained in the inflamed joint capsule of rats for more than 2 weeks (Figure S19, Supporting Information). Rats in the model group showed significantly higher levels of TNF- $\alpha$ , IL-1 $\beta$ , IL-6, and MCP-1 in the joint capsule (Figure 7b–e). These proinflammatory

cytokines significantly decreased after treatment with DEX/AHCPA NPs by intra-articular injection, as compared to other formulations. Moreover, local inflammation and cartilage erosion were evaluated by examining joint capsule sections stained with H&E or Safranin O/Fast Green. Notable inflammatory infiltrates as well as severe degradation and extensive loss of cartilage were observed in the model group. Mice treated with DEX/AHCPA NPs showed low levels of inflammatory cell infiltration as well as smooth and intact cartilage (Figure 7f). Compared with free DEX, the triggerable nanotherapy more effectively inhibited articular inflammation.

Together, these results demonstrated that the transformable nanotherapy derived from pH-responsive AHCPA NPs can be used for local treatment of inflammatory diseases by in situ gelation and sustaining drug release. It is worth noting that blank AHCPA NPs also showed varied degrees of efficacies, as implicated by the significantly decreased expressions of inflammatory cytokines in the examined two models of inflammatory diseases. For periodontitis, this should be due to in situ

formation of hydrogel in the periodontal pocket, which may act as a physical barrier to prevent bacterial invasion and reduce food residues.<sup>[20]</sup> In the case of arthritis, the locally formed hydrogel by AHCPA NPs can serve as a lubricant to reduce tissue damage. Indeed, rationally designed lubricating polymers can enhance cartilage regeneration in rats with early osteoarthritis.<sup>[21]</sup> Whereas transformable nanoparticles have been developed as triggerable nanotherapies or nanovaccines for cancer therapy most recently,<sup>[22]</sup> our studies, for the first time, demonstrated that rationally engineered hydrogel-transforming nanoparticles can be used for tissue protection and drug delivery for the treatment of diverse inflammatory diseases.

### 2.7. In Vivo Safety Studies

Finally, preliminary in vivo studies were conducted to evaluate safety profiles of the pH-responsive transformable nanoparticles. After oral gavage of AHCPA NPs at 2 or 5 g kg<sup>-1</sup> in mice, all animals remained healthy and displayed normal body weight gain during the experiment, without vomiting or diarrhea (Figure S20a, Supporting Information). After 2 weeks, all sacrificed mice exhibited comparable organ indices (Figure S20b, Supporting Information). There were no significant changes in the levels of red blood cells, hemoglobin, platelets, and white blood cells (Figure S20c–f, Supporting Information). Further quantification of biochemical markers including alanine aminotransferase, aspartate aminotransferase, blood urea, and creatinine suggested that orally delivered high-dose AHCPA NPs did not lead to injury to the liver and kidneys (Figure S20g–j, Supporting Information). Likewise, examination on H&E-stained sections of major organs revealed normal microstructure for AHCPA-NP-treated mice (Figure S21, Supporting Information). In separate studies, AHCPA NPs were administered in mice via subcutaneous injection. Luminescence imaging indicated that local administration of transformable nanoparticles did not induce inflammation or oxidative stress, which was comparable to those treated with saline (Figure S22, Supporting Information). Consequently, these preliminary results indicated that our transformable nanoparticles displayed good safety after oral delivery or local injection at relative high doses.

### 3. Conclusion

In summary, we engineered transformable nanoparticles by self-assembly of a pH-responsive multivalent cyclodextrin host material and a multivalent guest polymer, which can transform into hydrogels in response to acidic microenvironments, due to proton-mediated hydrolysis of the host material, generation of a hydrophilic multivalent host compound, and subsequently enhanced host–guest interactions. After oral delivery, the transformable nanoparticles can protect the stomach from ethanol- or drug-induced injury in mice, by generating a hydrogel barrier on the mucosa. In addition, these nanoparticles can function as responsive and transformable nanovehicles for various therapeutic agents to realize triggerable and sustained drug delivery, thereby effectively treating different inflammatory diseases.

This type of nanoparticle-transformed hydrogels own combined advantages of nanoparticles and hydrogels, such as good injectability, efficient loading capacity for hydrophobic/hydrophilic drugs and therapeutic cells, excellent stimuli-responsive cargo release performance, and desirable processibility to shape the final architecture. In combination with good in vivo safety, our pH-responsive, hydrogel-transformable nanoparticles hold great potentials in multiple biomedical applications, such as drug delivery, cell therapy, and tissue regeneration. It is worth noting that other pathologically relevant triggers such as abnormally overproduced reactive oxygen species and enzymes can also be employed for rational design of hydrogel-transformable nanoparticles to achieve advanced functionalities.

### Supporting Information

Supporting Information is available from the Wiley Online Library or from the author.

### Acknowledgements

Z.M.L. and G.L. contributed equally to this work. This study was supported by the National Natural Science Foundation of China (Grant Nos. 81971727 and 31670971), the National Key R&D Program of China (Grant No. 2018YFC1105302), the Double First Class University Plan of Zhejiang University, and the Program for Distinguished Young Scholars of TMMU. All animal experiments were performed in line with the Guide for the Care and Use of Laboratory Animals proposed by National Institutes of Health. All procedures and protocols were approved by the Animal Ethics Committee at Third Military Medical University (Chongqing, China), approval No.: AMUWEC2019122.

### Conflict of Interest

The authors declare no conflict of interest.

### Data Availability Statement

The data that support the findings of this study are available from the corresponding author upon reasonable request.

### Keywords

drug delivery, host–guest interactions, inflammatory diseases, responsive hydrogel, transformable nanoparticles

Received: November 13, 2021

Revised: February 10, 2022

Published online:

- [1] a) Y. S. Zhang, A. Khademhosseini, *Science* **2017**, *356*, eaaf3627; b) C. Liu, N. Morimoto, L. Jiang, S. Kawahara, T. Noritomi, H. Yokoyama, K. Mayumi, K. Ito, *Science* **2021**, *372*, 1078; c) D. Seliktar, *Science* **2012**, *336*, 1124; d) A. C. Daly, L. Riley, T. Segura, J. A. Burdick, *Nat. Rev. Mater.* **2020**, *5*, 20; e) J. Liu, S. Qu, Z. Suo, W. Yang, *Natl. Sci. Rev.* **2021**, *8*, nwa254; f) W. Lin,

- M. Kluzek, N. Iuster, E. Shimon, N. Kampf, R. Goldberg, J. Klein, *Science* **2020**, 370, 335; g) D. Y. Xia, P. Wang, X. F. Ji, N. M. Khashab, J. L. Sessler, F. H. Huang, *Chem. Rev.* **2020**, 120, 6070; h) H. Yuk, B. Y. Lu, X. H. Zhao, *Chem. Soc. Rev.* **2019**, 48, 1642; i) C. M. Madl, S. C. Heilshorn, H. M. Blau, *Nature* **2018**, 557, 335.
- [2] a) M. Vázquez-González, I. Willner, *Angew. Chem., Int. Ed.* **2020**, 59, 15342; b) N. Rauner, M. Meuris, M. Zoric, J. C. Tiller, *Nature* **2017**, 543, 407; c) P. H. J. Kouwer, M. Koepf, V. A. A. Le Sage, M. Jaspers, A. M. van Buul, Z. H. Eksteen-Akeroyd, T. Woltinge, E. Schwartz, H. J. Kitto, R. Hoogenboom, S. J. Picken, R. J. M. Nolte, E. Mendes, A. E. Rowan, *Nature* **2013**, 493, 651; d) L. Tang, L. Wang, X. Yang, Y. Y. Fen, Y. Li, W. Feng, *Prog. Mater. Sci.* **2021**, 115, 100702; e) S. Tang, B. M. Richardson, K. S. Anseth, *Prog. Mater. Sci.* **2021**, 120, 100738; f) A. M. Rosales, K. S. Anseth, *Nat. Rev. Mater.* **2016**, 1, 15012; g) Y. X. Dong, A. N. Ramey-Ward, K. Salaita, *Adv. Mater.* **2021**, 33, 2006600; h) X. Li, Y. B. Zhang, X. Y. Ren, Y. Wang, D. X. Chen, Q. Li, M. F. Huo, J. L. Shi, *Adv. Mater.* **2021**, 33, 2105348; i) J. L. Pelloth, P. A. Tran, A. Walther, A. S. Goldmann, H. Frisch, V. X. Truong, C. Barner-Kowollik, *Adv. Mater.* **2021**, 33, 2102184; j) L. Li, J. M. Scheiger, P. A. Levkin, *Adv. Mater.* **2019**, 31, 1807333.
- [3] a) B. Jiang, X. Liu, C. Yang, Z. Yang, J. Luo, S. Kou, K. Liu, F. Sun, *Sci. Adv.* **2020**, 6, eabc4824; b) S. Roberts, T. S. Harmon, J. L. Schaal, V. Miao, K. J. Li, A. Hunt, Y. Wen, T. G. Oas, J. H. Collier, R. V. Pappu, A. Chilkoti, *Nat. Mater.* **2018**, 17, 1154.
- [4] a) R. Dimatteo, N. J. Darling, T. Segura, *Adv. Drug Delivery Rev.* **2018**, 127, 167; b) L. J. Eggermont, Z. J. Rogers, T. Colombani, A. Memic, S. A. Bencherif, *Trends Biotechnol.* **2020**, 38, 418; c) M. A. English, L. R. Soenksen, R. V. Gayet, H. de Puig, N. M. Anagent-Mari, A. S. Mao, P. Q. Nguyen, J. J. Collins, *Science* **2019**, 365, 780; d) S. Q. Li, S. J. Dong, W. G. Xu, S. C. Tu, L. S. Yan, C. W. Zhao, J. X. Ding, X. S. Chen, *Adv. Sci.* **2018**, 5, 1700527; e) F. L. Mo, K. Jiang, D. Zhao, Y. Q. Wang, J. Song, W. H. Tan, *Adv. Drug Delivery Rev.* **2021**, 168, 79; f) B. P. Purcell, D. Lobb, M. B. Charati, S. M. Dorsey, R. J. Wade, K. N. Zellars, H. Doviak, S. Pettaway, C. B. Logdon, J. A. Shuman, P. D. Freels, J. H. Gorman3rd, R. C. Gorman, F. G. Spinale, J. A. Burdick, *Nat. Mater.* **2014**, 13, 653; g) W. Zhang, R. X. Wang, Z. M. Sun, X. W. Zhu, Q. Zhao, T. F. Zhang, A. Cholewinski, F. Yang, B. X. Zhao, R. Pinnaratip, P. K. Forooshani, B. P. Lee, *Chem. Soc. Rev.* **2020**, 49, 433; h) C. X. Fan, J. J. Shi, Y. Zhuang, L. L. Zhang, L. Huang, W. Yang, B. Chen, Y. Y. Chen, Z. F. Xiao, H. Shen, Y. N. Zhao, J. W. Dai, *Adv. Mater.* **2019**, 31, 1902900; i) P. M. Gawade, J. A. Shadish, B. A. Badeau, C. A. DeForest, *Adv. Mater.* **2019**, 31, 1902462; j) H. Madry, L. Gao, A. Rey-Rico, J. K. Venkatesan, K. Müller-Brandt, X. Cai, L. Goebel, G. Schmitt, S. Speicher-Mentges, D. Zurakowski, M. D. Menger, M. W. Laschke, M. Cucchiari, *Adv. Mater.* **2020**, 32, 1906508.
- [5] a) O. Chaudhuri, L. Gu, D. Klumpers, M. Darnell, S. A. Bencherif, J. C. Weaver, N. Huebsch, H.-P. Lee, E. Lippens, G. N. Duda, D. J. Mooney, *Nat. Mater.* **2016**, 15, 326; b) S. Talebian, M. Mehrli, N. Taebnia, C. P. Pennisi, F. B. Kadumudi, J. Foroughi, M. Hasany, M. Nikkhal, M. Akbari, G. Orive, A. Dolatshahi-Pirouz, *Adv. Sci.* **2019**, 6, 1801664; c) A. M. Kloxin, A. M. Kasko, C. N. Salinas, K. S. Anseth, *Science* **2009**, 324, 59; d) C. A. DeForest, K. S. Anseth, *Nat. Chem.* **2011**, 3, 925; e) T. E. Brown, K. S. Anseth, *Chem. Soc. Rev.* **2017**, 46, 6532.
- [6] a) D. R. Griffin, M. M. Archang, C.-H. Kuan, W. M. Weaver, J. S. Weinstein, A. C. Feng, A. Ruccia, E. Sideris, V. Ragkousis, J. Koh, M. V. Plikus, D. Di Carlo, T. Segura, P. O. Scumpia, *Nat. Mater.* **2021**, 20, 560; b) X. Xu, X. Xia, K. Zhang, A. Rai, Z. Li, P. Zhao, K. Wei, L. Zou, B. Yang, W.-K. Wong, W.-Y. C. Philip, L. Bian, *Sci. Transl. Med.* **2020**, 12, eaba8014; c) Y. Wang, L. Li, Y. Ma, Y. Tang, Y. Zhao, Z. Li, W. Pu, B. Huang, X. Wen, X. Cao, J. Chen, W. Chen, Y. Zhou, J. Zhang, *ACS Nano* **2020**, 14, 8202; d) E. S. Sani, R. P. Lara, Z. Aldawood, S. H. Bassir, D. Nguyen, A. Kantarci, G. Intini, N. Annabi, *Matter* **2019**, 1, 926; e) B. Guo, R. Dong, Y. Liang, M. Li, *Nat. Rev. Chem.* **2021**, 5, 773; f) Z. J. Xu, S. Y. Han, Z. P. Gu, J. Wu, *Adv. Healthcare Mater.* **2020**, 9, 1901502; g) R. Z. Murray, Z. E. West, A. J. Cowin, B. L. Farrugia, *Burns Trauma* **2019**, 7, s41038; h) S. Nam, D. Mooney, *Chem. Rev.* **2021**, 121, 11336; i) F. Gelain, Z. L. Luo, S. G. Zhang, *Chem. Rev.* **2020**, 120, 13434; j) L. M. Stapleton, A. N. Steele, H. Wang, H. L. Hernandez, A. C. Yu, M. J. Paulsen, A. A. A. Smith, G. A. Roth, A. D. Thakore, H. J. Lucian, K. P. Totherow, S. W. Baker, Y. Tada, J. M. Farry, A. Eskandari, C. E. Hironaka, K. J. Jaatinen, K. M. Williams, H. Bergamasco, C. Marschel, B. Chadwick, F. Grady, M. Ma, E. A. Appel, Y. J. Woo, *Nat. Biomed. Eng.* **2019**, 3, 611; k) J. Yu, K. Wang, C. C. Fan, X. Y. Zhao, J. S. Gao, W. H. Jing, X. P. Zhang, J. Li, Y. Li, J. H. Yang, W. G. Liu, *Adv. Mater.* **2021**, 33, 2008395.
- [7] E. Prince, E. Kumacheva, *Nat. Rev. Mater.* **2019**, 4, 99.
- [8] a) J. X. Zhang, P. X. Ma, *Adv. Drug Delivery Rev.* **2013**, 65, 1215; b) J. Guo, H. Tao, Y. Dou, L. Li, X. Xu, Q. Zhang, J. Cheng, S. Han, J. Huang, X. Li, X. Li, J. Zhang, *Mater. Today* **2017**, 20, 493; c) J. Zhang, P. X. Ma, *Nano Today* **2010**, 5, 337; d) S. Han, S. Chen, L. Li, J. Li, H. An, H. Tao, Y. Jia, S. Lu, R. Wang, J. Zhang, *ACS Cent. Sci.* **2018**, 4, 600; e) G. Yang, P. Wu, C. Yu, J. Zhang, J. Song, *ChemistrySelect* **2020**, 5, 8707; f) Q. Zhang, F. Zhang, S. Li, R. Liu, T. Jin, Y. Dou, Z. Zhou, J. Zhang, *Theranostics* **2019**, 9, 3732; g) C. Li, Y. Zhao, J. Cheng, J. Guo, Q. Zhang, X. Zhang, J. Ren, F. Wang, J. Huang, H. Hu, R. Wang, J. Zhang, *Adv. Sci.* **2019**, 6, 1900610.
- [9] a) J. Zhang, Y. Jia, X. Li, Y. Hu, X. Li, *Adv. Mater.* **2011**, 23, 3035; b) K. E. Broaders, J. A. Cohen, T. T. Beaudette, E. M. Bachelder, J. M. Fréchet, *Proc. Natl. Acad. Sci. USA* **2009**, 106, 5497.
- [10] M. V. Rekharsky, Y. Inoue, *Chem. Rev.* **1998**, 98, 1875.
- [11] a) C.-M. Lehr, F. G. J. Poelma, H. E. Junginger, J. J. Tukker, *Int. J. Pharm.* **1991**, 70, 235; b) G. Fuhrmann, A. Grotzky, R. Lukic, S. Matoori, P. Luciani, H. Yu, B. Zhang, P. Walde, A. D. Schlüter, M. A. Gauthier, J.-C. Leroux, *Nat. Chem.* **2013**, 5, 582.
- [12] S. K. Lai, Y. Y. Wang, J. Hanes, *Adv. Drug Delivery Rev.* **2009**, 61, 158.
- [13] a) F. Hugenholtz, W. M. de Vos, *Cell. Mol. Life Sci.* **2018**, 75, 149; b) E. L. McConnell, A. W. Basit, S. Murdan, *J. Pharm. Pharmacol.* **2008**, 60, 63.
- [14] a) S. Lucas, *Headache* **2016**, 56, 436; b) L. Laine, R. Smith, K. Min, C. Chen, R. W. Dubois, *Aliment. Pharmacol. Ther.* **2006**, 24, 751; c) S. Nalamachu, R. Wortmann, *Postgrad. Med.* **2014**, 126, 92.
- [15] Y. Dou, C. Li, L. Li, J. Guo, J. Zhang, *J. Controlled Release* **2020**, 327, 641.
- [16] D. F. Kinane, P. G. Stathopoulou, P. N. Papapanou, *Nat. Rev. Dis. Primers* **2017**, 3, 17038.
- [17] J. Marchesan, M. S. Ginary, L. Jing, M. Z. Miao, S. Zhang, L. Sun, T. Morelli, M. H. Schoenfish, N. Inohara, S. Offenbacher, Y. Jiao, *Nat. Protoc.* **2018**, 13, 2247.
- [18] a) M. Agnello, L. Cen, N. C. Tran, W. Shi, J. S. McLean, X. He, *J. Dent. Res.* **2017**, 96, 924; b) A. F. Paes Leme, H. Koo, C. M. Bellato, G. Bedi, J. A. Cury, *J. Dent. Res.* **2006**, 85, 878.
- [19] a) M. Farr, K. Garvey, A. M. Bold, M. J. Kendall, P. A. Bacon, *Clin. Exp. Rheumatol.* **1985**, 3, 99; b) P. Geborek, T. Saxne, H. Pettersson, F. A. Wollheim, *J. Rheumatol.* **1989**, 16, 468; c) N. A. Cummings, G. L. Nordby, *Arthritis Rheum.* **1966**, 9, 47; d) P. S. Treuhaft, D. J. McCarty, *Arthritis Rheum.* **1971**, 14, 475; e) T. T. Ward, R. T. Steigbigel, *Am. J. Med.* **1978**, 64, 933.
- [20] Y. Almoshari, R. Ren, H. Zhang, Z. Jia, X. Wei, N. Chen, G. Li, S. Ryu, S. M. Lele, R. A. Reinhardt, D. Wang, *Biomaterials* **2020**, 261, 120293.
- [21] R. Xie, H. Yao, A. S. Mao, Y. Zhu, D. Qi, Y. Jia, M. Gao, Y. Chen, L. Wang, D.-A. Wang, K. Wang, S. Liu, L. Ren, C. Mao, *Nat. Biomed. Eng.* **2021**, 5, 1189.
- [22] a) N. Gong, Y. Zhang, X. Teng, Y. Wang, S. Huo, G. Qing, Q. Ni, X. Li, J. Wang, X. Ye, T. Zhang, S. Chen, Y. Wang, J. Yu, P. C. Wang, Y. Gan, J. Zhang, M. J. Mitchell, J. Li, X.-J. Liang, *Nat. Nanotechnol.* **2020**, 15, 1053; b) L. Zhang, D. Jing, N. Jiang, T. Rojalin, C. M. Baehr, D. Zhang, W. Xiao, Y. Wu, Z. Cong, J. J. Li, Y. Li, L. Wang, K. S. Lam, *Nat. Nanotechnol.* **2020**, 15, 145.